

Synergistic Inhibition between Sodium Dietyldithiocarbamate and Hexadecyltrimethylammonium Bromide on the Corrosion of Cold Rolled Steel in Acetic Acid

*You Wu, Yu-Lu Shi, Chang-Wei Su, Li-Li Feng, Jun-Ming Guo, Wei Bai**

Key Laboratory of Resource Clean Conversions in Ethnic Regions, Yunnan Minzu University, Kunming, 650500, PR China

*E-mail: bw369852147@qq.com

Received: 31 May 2017 / Accepted: 15 September 2017 / Published: 12 October 2017

Weight loss method, potentiodynamic polarization and electrochemical impedance spectroscopy (EIS) were used to study the synergistic inhibition effect of sodium dietyldithiocarbamate (DDTC) and hexadecyltrimethylammonium bromide (CTAB) for the corrosion of cold rolled steel (CRS) in 0.05 M acetic acid (HAc) solution. It is observed that the combination between DDTC and CTAB is physically adsorbed on the surface of CRS, thus showing excellent inhibition efficiency. In this article, the Hard-Soft Acid-Base (HSAB) principle has used to explain the mechanisms of Synergistic inhibition between DDTC and CTAB. SEM and FT-IR results further validate the corrosion inhibition mechanism we proposed.

Keywords: Cold rolled steel; Corrosion; HAc; Synergistic inhibition effect

1. INTRODUCTION

Acetic acid (HAc) is a weak organic acid, which has a long history of usage as solvents or chemical raw materials in producing of industry such as chemical engineering, textile, light industry, medicine and food. It also is widely used in acid cleaning, industry cleaning, acid dipping, and removal of furring [1,2]. The consumption of acetic acid is higher than that of other organic acids. The status of acetic acid in organic chemical industry is comparable to that of sulfuric acid in inorganic chemical industry [3]. Carbon steels are the most commonly used materials in industrial production, but they are very prone to corrosion in environments containing HAc [4]. The addition of inhibitors is a method to solve the difficult problem of carbon steel used in acetic acid environment, and its research has attracted people's attention [5].

Inhibitors are usually used to control the corrosion processes of the metal. Inhibitors are compounds that control, reduce, or prevent reactions between a metal and its surroundings when added to the medium in small quantities [6]. But because of its high synthesis conditions, more steps and product separation difficulties lead to its use of high cost, thus limiting the practical application of inhibitors. Surfactant with nitrogen groups were considered to be one of effective chemicals for inhibiting the corrosion of metals [7]. Previous studies on the synergistic effect of surfactants have focused on inorganic strong acid systems, and mainly studied the synergistic corrosion inhibition of surfactants and halide ions [8-13]. However, little has been written about the synergistic inhibition of cold rolled steel in the presence of HAc solutions. The corrosion mechanism of carbon steel in HAc is very complicated, because of the HAc would introduce additional factors to further complicate the corrosion processes [14-16].

In this work, the synergistic inhibition between sodium diethyldithiocarbamate (DDTC) and hexadecyltrimethylammonium bromide (CTAB) on the corrosion of cold rolled steel in 0.05 M acetic acid media is studied by weight loss, potentiodynamic polarization, electrochemical impedance spectroscopy (EIS) and surface analysis methods. Meanwhile, probable inhibitive mechanisms are presented to explain the experimental observation.

2. EXPERIMENTAL

2.1. Material

The working electrodes were made of a sheet of cold rolled steel, which was of commercial specification with composition (wt %):

C \leq 0.10%, Mn \leq 0.50%, S \leq 0.025%, P \leq 0.025%, Fe remainder.

2.2. Solutions

Acetic acid (HAc), DDTC, and CTAB used were of analytical grade. All solutions were prepared from distilled water.

2.3. Weight loss measurements

Weight loss tests were conducted under total immersion conditions 250 ml of test solution (0.05 M HAc without and with inhibitors) maintained at 30 °C controlled by water thermostat. Three parallel CRS sheets of 4.0 cm \times 1.5 cm \times 0.06 cm were abraded by a series of emery paper (grade 100-400-600-800-1000) and then washed with distilled water and acetone. After weighing accurately by METTLER TOLEDO, the specimens were suspended in a beaker containing test solutions using nylon lines and wood rods. The exposed total surface area of each specimen is 12.5 cm². The specimens were taken from test solutions after immersion for 72 h, washed under running water in order to remove the corrosion product, dried with a hot air stream, and re-weighed accurately. The mean weight loss of

three parallel CRS sheets was obtained and reported. The inhibition efficiency (IE_w) is calculated as follows:

$$IE_w \% = \frac{W_0 - W}{W_0} \times 100\% \quad (1)$$

Where W_0 and W are the values of average weight loss of three parallel CRS sheets without and with inhibitors, respectively.

2.4. Electrochemical measurements

Electrochemical experiments were carried out in the typical three-electrode cell with a working electrode (WE), an auxiliary electrode (CE) and a reference electrode (RE). The working electrodes were made of cold rolled steel specimen which was embedded in PVC holder using epoxy resin with a square surface of 1.0 cm^2 .

Each sample was successively polished using SiC emery papers from 100 to 1000 grades on the test face, then rinsed with distilled water, degreased with acetone (CH_3COCH_3), and dried with a hot air stream. The auxiliary electrode is a platinum foil and the reference electrode is a saturated calomel electrode (SCE) with a fine Luggin capillary positioned close to the working electrode surface in order to minimize ohmic potential drop. The working electrode was immersed in the test solution at open circuit potential for 2 h before measurement until a steady state appeared. All the potentials reported here were measured against the saturated calomel electrode. To obtain the Tafel plots, polarization curves were performed by polarizing to $\pm 250 \text{ mV}$ with respect to the free corrosion potential (E_{corr}) at a scan rate of 0.5 mV/s . All electrochemical measurements were carried out using CS350 (Electrochemical Work station) advanced electrochemical system. Each experiment was repeated at least three times to check the reproducibility. [17] The test solutions were maintained at $30 \text{ }^\circ\text{C}$ controlled by water thermostat. Inhibition efficiency ($E_p \%$) is defined as:

$$IE_p \% = \frac{I_{\text{corr}} - I_{\text{corr(inh)}}}{I_{\text{corr}}} \times 100\% \quad (2)$$

Where I_{corr} and $I_{\text{corr(inh)}}$ represent corrosion current density values without and with inhibitor, respectively.

Electrochemical impedance spectroscopy (EIS) carried out at E_{ocp} in the frequency range of 10^1 Hz to 10^5 Hz using 10 mV peak-to-peak voltage excitation. Inhibition efficiency ($IE_{Rt} \%$) is calculated by the following equation:

$$IE_{Rt} \% = \frac{R_{t(\text{inh})} - R_{t(0)}}{R_{t(\text{inh})}} \times 100\% \quad (3)$$

Where $R_{t(0)}$ and $R_{t(\text{inh})}$ are charge transfer resistance values for CRS in the absence and presence of inhibitor, respectively.

2.5. SEM analysis

The CRS sheets ($1 \times 1 \times 0.5 \text{ cm}$) were abraded by a series of emery paper (grade 100-400-600-800-1000) and then washed with distilled water and acetone, dried with a blower. Then the sheets were

suspended in the test solution at 30°C for 6h, their surface characteristics and corrosion features were examined by FEI Quanta 650 scanning electron microscopy (SEM).

2.6. FT-IR analysis

In order to confirm the adsorption type of the CTAB and DDTC after synergized, Nicolet iS5N FT-IR was used to measure the spectra of the corroded surface, all the spectra in these experiments were obtained in the region from 400 to 4000 cm^{-1} .

3. RESULTS AND DISCUSSION

3.1 Weight loss measurements

Use of weight loss techniques of evaluating inhibition efficiency is reliability [18-20]. In this present study, the reproducibility of results obtained percentage inhibition efficiency values for triplicate determination was very precise.

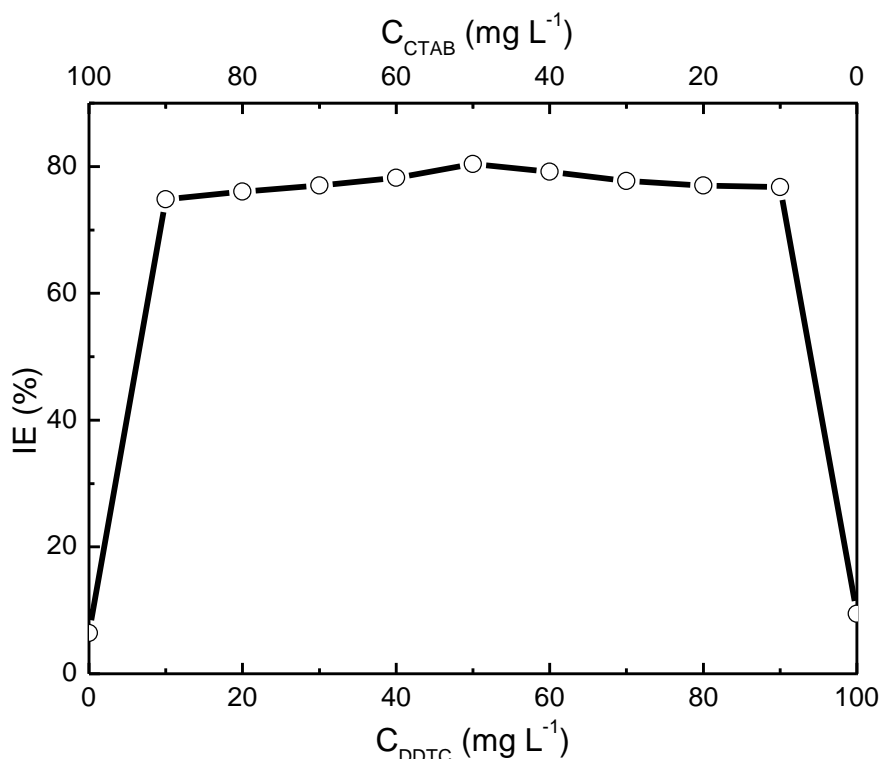


Figure 1. Relationship between inhibition efficiency (IE_w) obtained from weight loss method and concentration of different ratio $C_{\text{DDTC}}/C_{\text{CTAB}}$ in 0.05 M HAc at 30°C (immersion time is 72h, surface area is 12.5 cm^2).

Fig.1 shows the values of inhibition efficiency obtained from the weight loss (W) for inhibitor concentration of different ratio $C_{\text{DDTC}}/C_{\text{CTAB}}$ in 0.05 M HAc at 30°C. As can be seen from Fig.1, the addition of the DDTC-CTAB mixture to aggressive media is accompanied by an increase of the

inhibition efficiency, as compared to the blank solution, the solution with 50mg/L DDTC or the solution with 50mg/L CTAB only. This behavior can be explained by the formation of the more resistant and adhered protective film on the cooled rolled steel’s surface, as compared to that formed in the presence of the DDTC or CTAB only. The highest inhibition efficiency was obtained in the formulation consisting of 50 mg/L DDTC and 50 mg/L CTAB.

The results obtained using the weight loss method suggests a synergic effect between DDTC and CTAB.

3.2. Polarization studies

The cathodic and anodic polarization curves for CRS in 0.05 M HAc in the presence of 50 mg/LCTAB, 50 mg/L DDTC and 50 mg/LCTAB+50 mg/L DDTC were shown in Fig.2. Fig. 2 clearly shows that comparing the absence of inhibitor, the corrosion potentials are shifted to more positive potential direction in the presence of inhibitor which indicates that the combination of CTAB and DDTC acts as anodic type inhibitor.

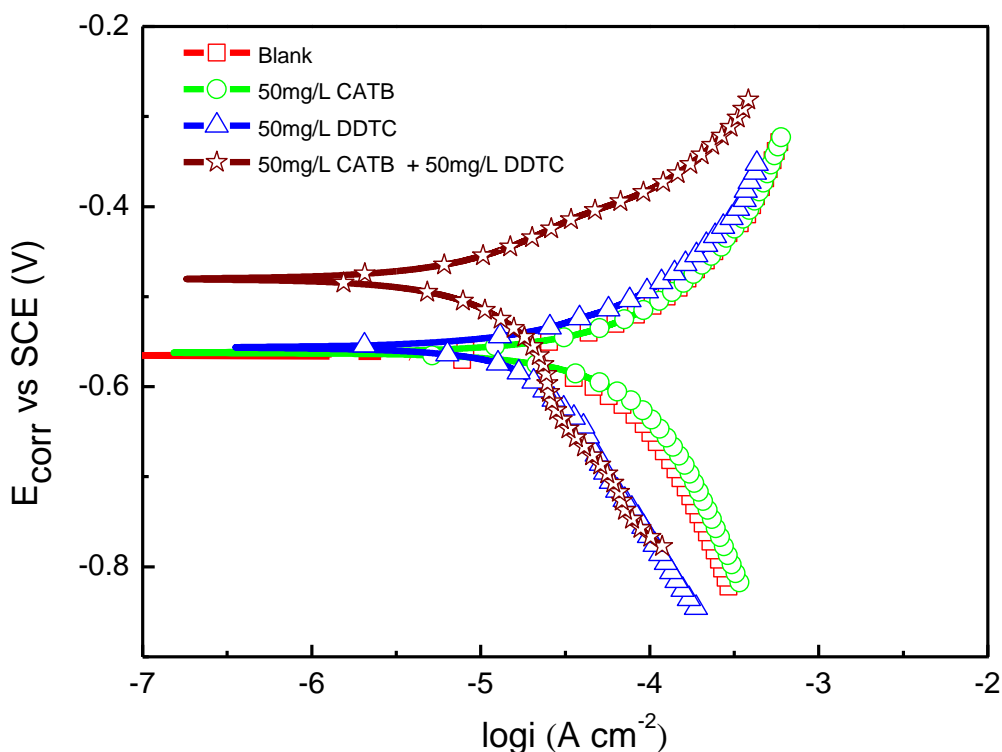


Figure 2. Polarization curves for CRS in 0.05 M HAc with and without CTAB and DDTC at 30°C.

The potentiodynamic polarization parameters including corrosion potential (E_{corr}), corrosion current densities (I_{corr}) calculated by Tafel plots, anodic Tafel slope (b_a), cathodic Tafel slope (b_c), inhibition efficiencies (IE_p) calculated using the equations (2) for the corrosion of cold rolled steel in 0.05 M HAc at 30°C with inhibitors of DDTC or CTAB, between DDTC and CTAB were listed in the Table 1.

Table 1. Electrochemical parameters from Tafel polarization curves and inhibition efficiencies in 0.05 M HAc at 30 °C

C / mg/L	b_a / mV/decade	b_c / mV/decade	i_{corr} / $\text{mA}\cdot\text{cm}^{-2}$	E_{corr} / mV	IE_p / %
Blank	70.33	93.08	0.0290	-565.87	—
50mg/L CTAB	74.97	86.03	0.0263	-562.62	9.31
50mg/L DDTC	59.54	122.44	0.0159	-558.02	45.17
50mg/LCTAB+50mg/LDDTC	68.82	95.86	0.0062	-480.9	78.62

As can be seen from Table1, when the addition of CTAB-DDTC mixture in pilot medium is accompanied by a shift of the current density (i_{corr}) towards the negative values. The analysis of the results obtained shows that the presence of the CTAB-DDTC mixture, the corrosion potential (E_{corr}) is displaced in the positive direction from -565.87 to -480.9 mV; the current density decreases from 0.029 to 0.0062 mA/cm². Accordingly, inhibition efficiency (IE_p) values increase from 0 % to 78.62 %. The results are in good agreement that obtained from weight loss technique.

The i_{corr} values for CRS in 0.05 M HAc with between CTAB and DDTC at different temperatures were shown in Fig. 3.

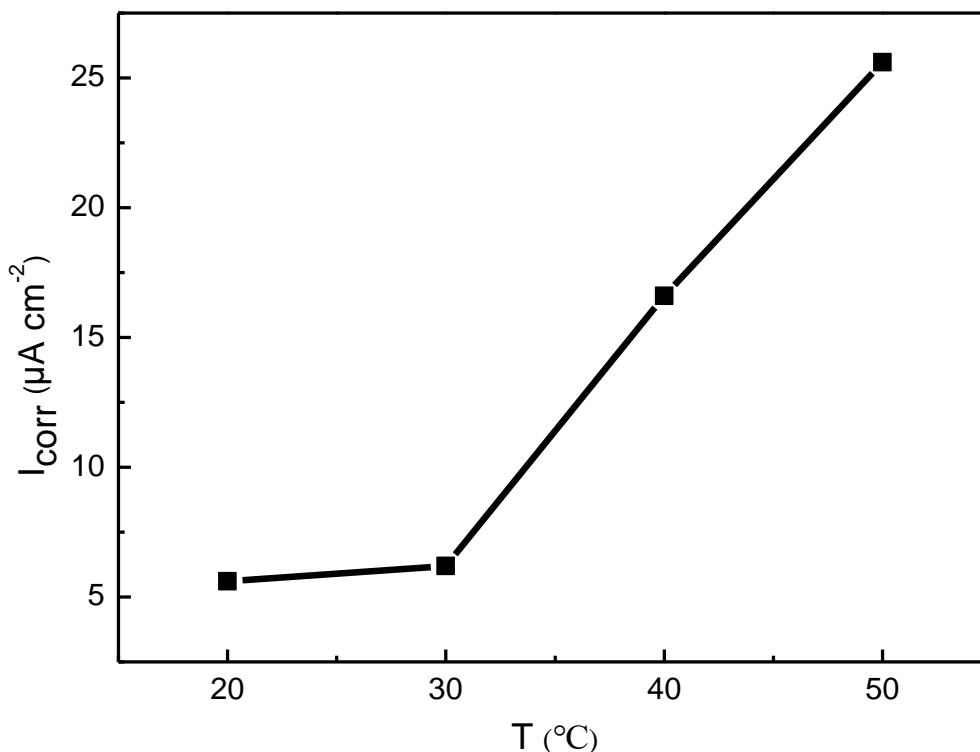


Figure 3. I_{corr} for CRS in 0.05 M HAc with between CTAB and DDTC at different temperatures.

Fig. 3 shows that, the i_{corr} values increases with the increase of temperature in the presence of between CTAB and DDTC. This shows that with the increase of temperature, the degree of adsorption of CTAB-DDTC on the surface of CRS is more and more weak, resulting in increased corrosion of CRS. We believe that CTAB and DDTC after synergized are adsorbed on the surface of CRS in the form of physical adsorption.

3.3. EIS

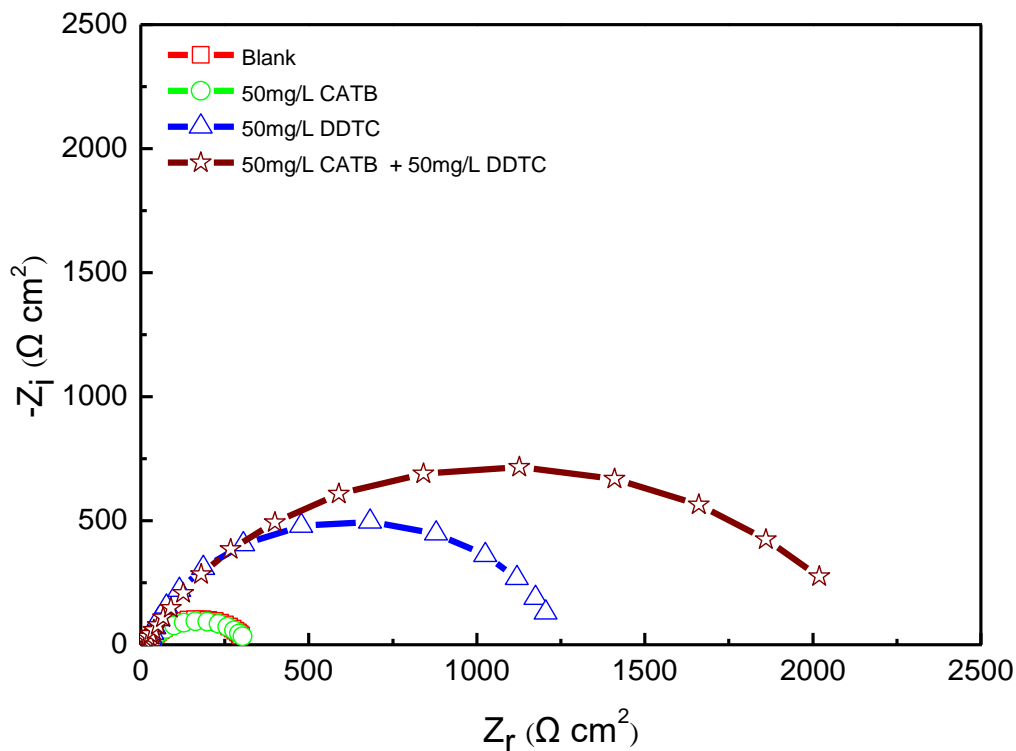


Figure 4. Nyquist plots for CRS in 0.05 M HAc solution with and without CTAB and DDTC at 30°C.

Fig. 4 shows the Nyquist plots for cold rolled steel in 0.05 M HAc at 30 °C containing blank, 50 mg/LCTAB, 50 mg/L DDTC and 50 mg/LCTAB+50 mg/L DDTC, respectively. All the impedance spectra exhibit one single depressed semicircle, and the diameter of semicircle increases from blank, 50 mg/LCTAB, 50 mg/L DDTC to 50 mg/LCTAB-50 mg/L DDTC, which suggests that the combination between DDTC and CTAB shows excellent inhibition efficiency. The single semicircle indicates that the charge transfer takes place at electrode/solution interface, and the transfer process controls corrosion reaction of steel and the presence of inhibitor does not change the mechanism of steel dissolution [21]. Also, it is clear from these figures that the impedance diagrams are not perfect semicircles which can be attributed to the frequency dispersion as a result of roughness and in homogeneousness of the electrode surface [22-24].

The EIS results were simulated using the equivalent circuit shown in Fig. 5 to pure electronic models that could verify or rule out mechanistic models and enable the calculation of numerical values corresponding to the physical and/or chemical properties of the electrochemical system under investigation [25]. The circuit employed (Fig.5) allows the identification of both solution resistance (R_s) and charge transfer resistance (R_t). It is important to mention that the double layer capacitance value is affected by imperfections of the surface, and that this effect is simulated via a constant phase element (CPE) [26]. In this work, the electrochemical parameters including charge transfer resistance (R_t) and constant phase element (CPE) obtained by fitting the spectra using the Zview, are given in

Table 2. The inhibition efficiencies (IE_{R_t}) from R_t for the corrosion of steel were calculated and also listed in Table 2 by means of the equation (3).

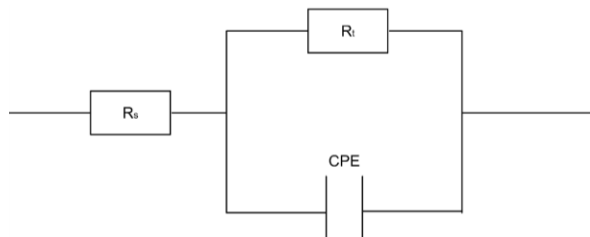


Figure 5. Equivalent circuit used to fit the EIS data of cold rolled steel in 0.05 M HAc with and without inhibitor.

Table 2. EIS parameters for the corrosion of CRS in 0.05 M HAc solution with and without CTAB and DDTC at 30°C.

C (mg/L)	R_s (Ω cm^2)	R_t (Ω cm^2)	CPE-T (μF cm^2)	CPE-P	IE_{R_t} %
Blank	522.1	296.2	199	0.76	—
50mg/LCTAB	474.2	302.3	190	0.76	2.02
50mg/LDDTC	474.2	1225	139	0.87	75.82
50mg/LCTAB+50mg/LDDTC	381	2160	119	0.75	86.29

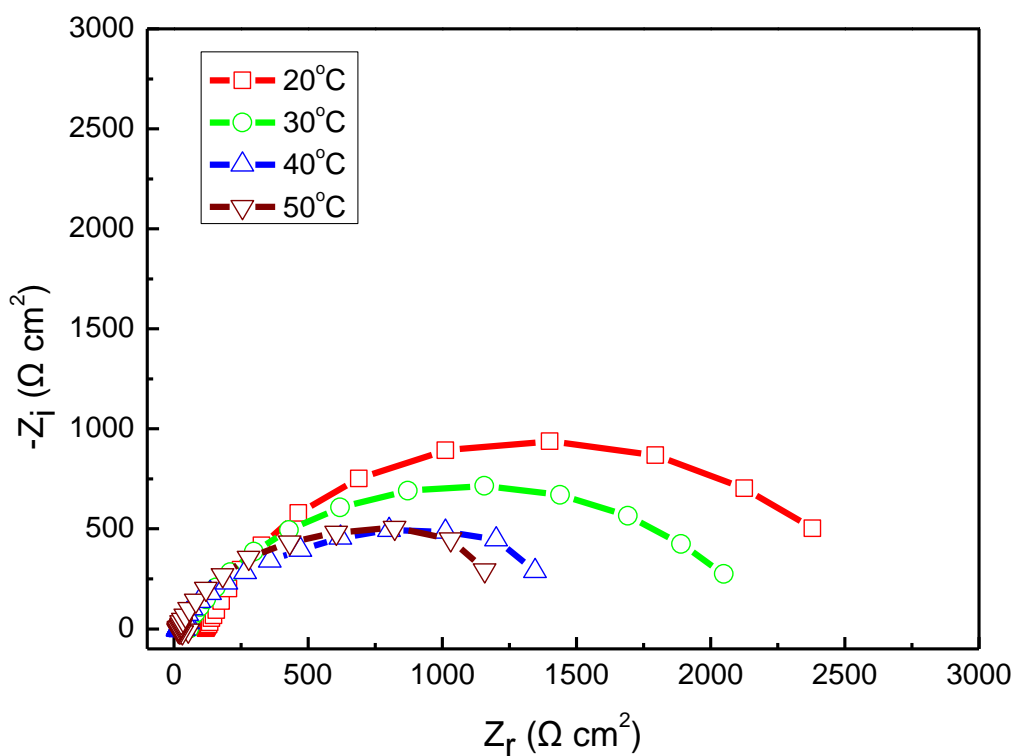


Figure 6. Nyquist plots for CRS in 0.05 M HAc with between CTAB and DDTC at different temperatures.

Fig.6 shows the Nyquist plots for CRS in 0.05 M HAc with between CTAB and DDTC at different temperatures. In Fig. 6, the capacitive arc with increasing temperature becomes small, and the shape does not change. This shows that with the increase of temperature, the degree of adsorption of CTAB-DDTC on the surface of CRS is more and more weak, resulting in increased corrosion of CRS. This is consistent with the analyses above, that CTAB and DDTC after synergized are adsorbed on the surface of CRS in the form of physical adsorption.

3.4 SEM analysis

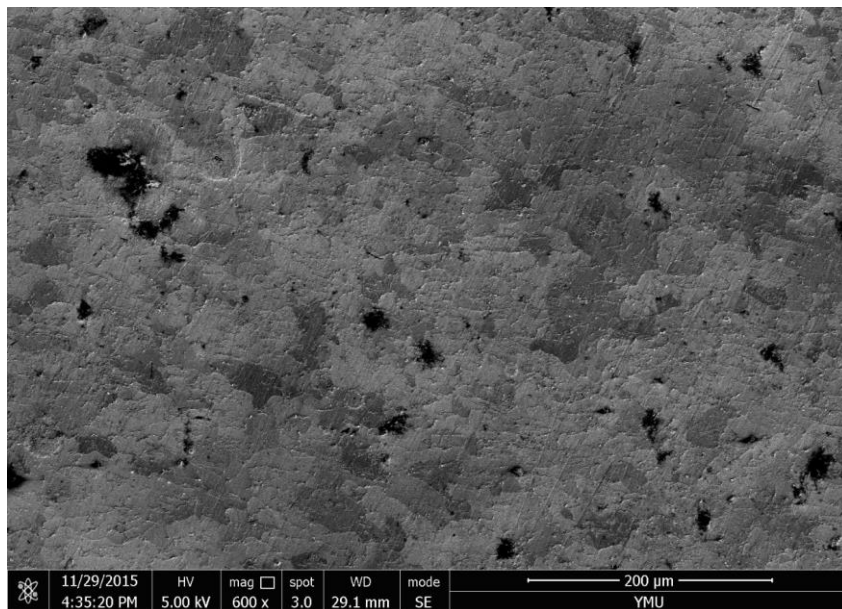


Figure 7. SEM examination of CRS surface after 6h immersion in 0.05 M HAc solution at 30°C.

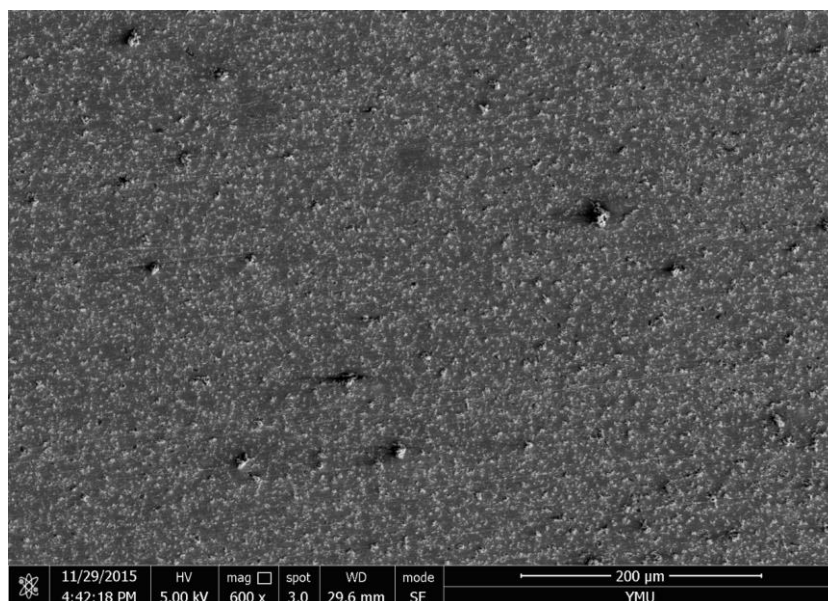


Figure 8. SEM examination of CRS surface after 6h immersion in 0.05 M HAc solution with CTAB at 30°C.

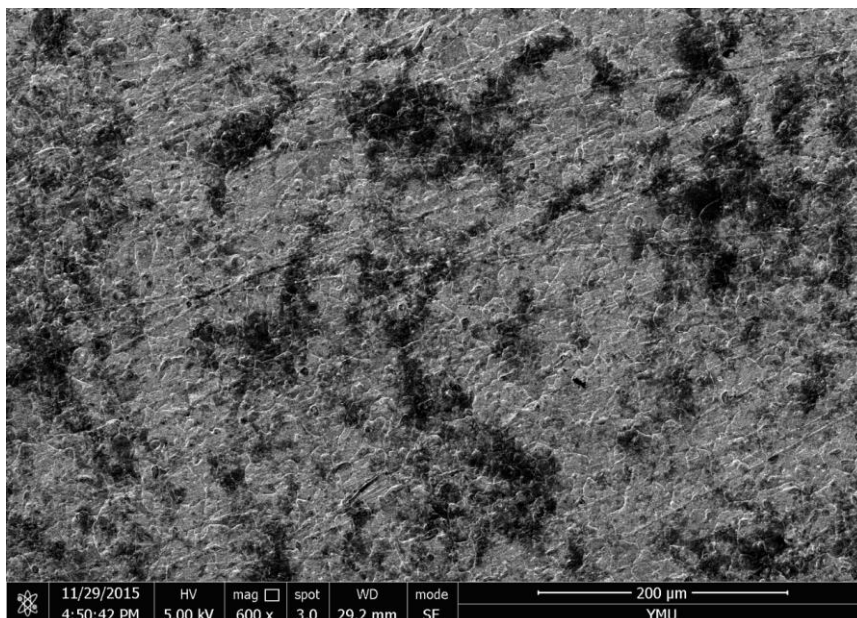


Figure 9. SEM examination of CRS surface after 6h immersion in 0.05 M HAc solution with DDTC at 30°C.

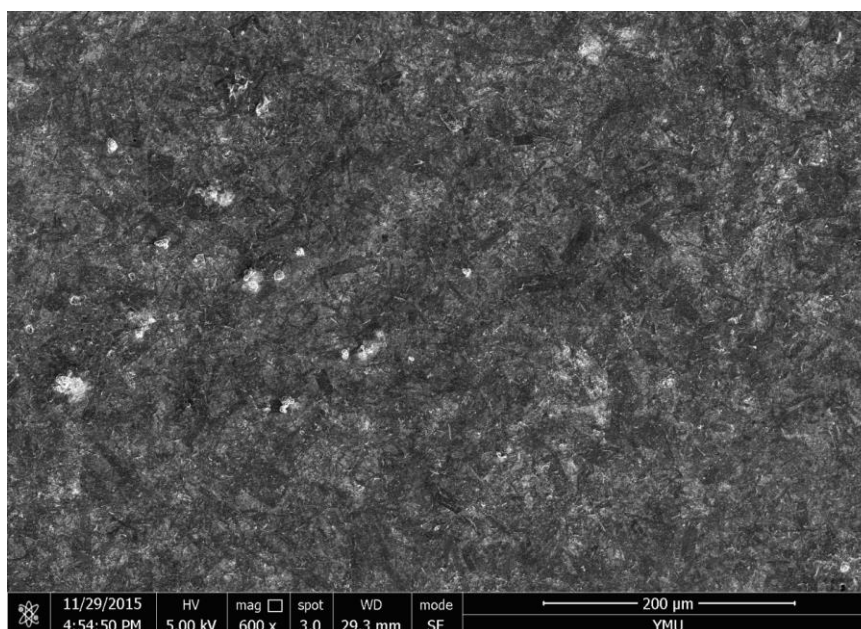


Figure 10. SEM examination of CRS surface after 6h immersion in 0.05 M HAc solution with CTAB and DDTC at 30°C.

Fig. 7 show the SEM microstructures of CRS surface after 6h immersion in 0.05 M HAc solution at 30°C, there were some pitting on the surfaces of CRS. Fig. 8 show the SEM microstructures of CRS surface after 6h immersion in 0.05 M HAc solution with CTAB at 30°C, Fig. 9 show the SEM microstructures of CRS surface after 6h immersion in 0.05 M HAc solution with DDTC at 30°C, the pitting layer in Fig. 9 is little than that in Fig.8 and far less than that in Fig. 7. Fig. 10 show the SEM microstructures of CRS surface after 6h immersion in 0.05 M HAc solution with CTAB and DDTC at

30°C. The presence of pitting was almost disappeared in Fig. 10. It is obviously to see from Fig. 10 that, there formed a layer of thick protective film cover on the surface of CRS, this layer protects the CRS from corrosion of acetic acid [27]. The thickness of the protective film in Fig. 10 is thicker than in Fig. 9 and Fig. 8, it is consistent with the results of electrochemical measurements.

3.5. FT-IR analysis

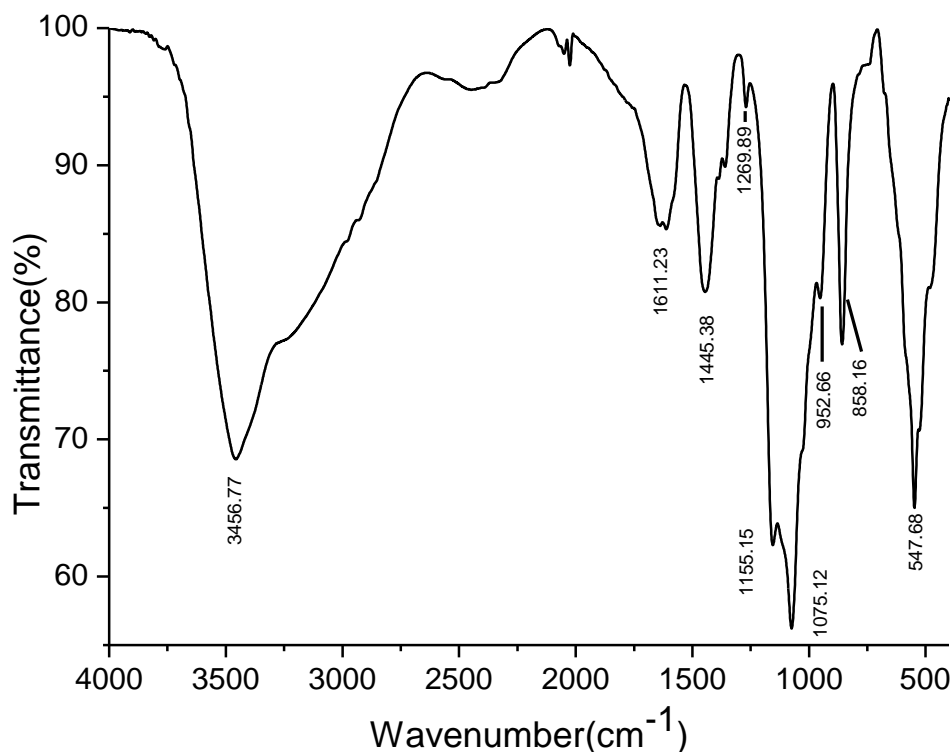


Figure 11. FT-IR spectra of the corrosion surfaces of CRS after 6h immersion in 0.05 M HAC solution at 30°C.

For confirming the adsorption type of the CTAB and DDTC after synergized, the FT-IR was used to characterize the products on the surface of CRS. Fig. 11 shows the FT-IR spectra of the corrosion surfaces of CRS after 6h immersion in 0.05 M HAC solution at 30°C. In Fig. 11, the broader band at 3456.77 cm^{-1} could be ascribed to the O-H stretching vibration. The peak at 1611.23 cm^{-1} results from the stretching vibration of C=O. The peak at 1445.38 cm^{-1} is attributed to CH₃ stretching vibration. The peaks at 1269.89 cm^{-1} , 1155.15 cm^{-1} and 1075.12 cm^{-1} are ascribed to the stretching vibration of C-O. There are characteristic absorption peaks of HAC at 952.66 cm^{-1} and 547.68 cm^{-1} . The peak at 858.16 cm^{-1} results from the stretching vibration of Fe-O. Fig. 12 shows the FT-IR spectra of the corrosion surfaces of CRS after 6h immersion in 0.05 M HAC solution with CTAB and DDTC at 30°C.

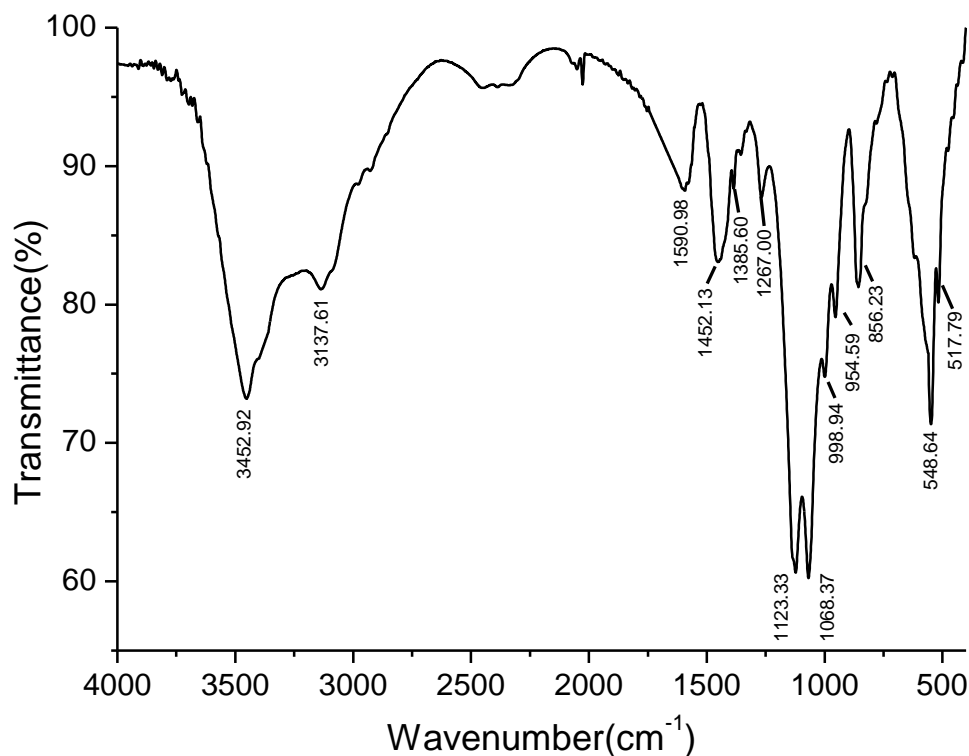


Figure 12. FT-IR spectra of the corrosion surfaces of CRS after 6h immersion in 0.05 M HAc solution with CTAB and DDTC at 30°C.

In Fig. 12, the broader band at 3452.92 cm^{-1} could be ascribed to the O-H stretching vibration. The peak at 3137.61 cm^{-1} results from the stretching vibration of CH₂. The peak at 1590.98 cm^{-1} results from the stretching vibration of C=O. The peak at 1452.13 cm^{-1} results from the stretching vibration of CH₃. The peak at 1385.60 cm^{-1} is attributed to C-N stretching vibration. The peaks at 1267.00 cm^{-1} , 1123.33 cm^{-1} and 1068.37 cm^{-1} are ascribed to the stretching vibration of C-O [28]. The peak at 998.94 cm^{-1} is attributed to C=S stretching vibration. There are characteristic absorption peaks of HAc at 954.59 cm^{-1} and 548.64 cm^{-1} . The peak at 856.23 cm^{-1} results from the stretching vibration of Fe-O. The peak at 517.79 cm^{-1} is attributed to C-S stretching vibration. In Fig. 12, it is shown that the spectrum may be red-shifted and blue-shifted in comparison with the spectrum in Fig. 11. The new functional group such as C-N, CH₂, C-S and C=S are come from CTAB and DDTC. In addition, there is no new functional group produced. We can conclude that CTAB and DDTC after synergized are adsorbed on the surface of CRS in the form of physical adsorption.

4. MECHANISM OF CORROSION INHIBITION

Pearson introduced the concept of hardness through his famous hard-soft acid-base (HSAB) principle which states that, “hard acids prefer to coordinate with hard bases and soft acids prefer to coordinate with soft bases for both their thermodynamic and kinetic properties” [29]. The surface of the cold rolled steel is positively charged in the acetic acid solution [30].

When added acetic acid, the surface of cold rolled steel(CRS) gathered a large number of Fe^{2+} , which impelled hard base CH_3COO^- preferentially adsorbed on the surface of the CRS than water dipole, forming a compact layer of $\text{CH}_3\text{COO}^- \cdot \text{H}_2\text{O}$. When CTAB was added, there was a competitive adsorption between Br^- in CTAB and CH_3COO^- . Although the interaction force between the hard base CH_3COO^- and the borderline acid Fe^{2+} is lower than that between the borderline base Br^- and the borderline acid Fe^{2+} , and Br^- broken through the water dipole layer and produced specific adsorption on the surface of CRS, the coverage of Br^- on the surface of CRS was still small because the number of CH_3COO^- is 364 times that of Br^- . In addition, the $\text{C}_{19}\text{H}_{42}\text{N}^+$ in CTAB repelled the surface of CRS which gathered a large number of Fe^{2+} , led to a larger molecular CTAB could not adsorb on the surface of CRS. The above reasons led to Br^- cannot play a guiding role, and therefore low rate of inhibition.

When DDTC was added, the interaction force between the hard base CH_3COO^- and the borderline acid Fe^{2+} is lower than that between the borderline base $(\text{C}_2\text{H}_5)_2\text{NCSS}^-$ in DDTC and the borderline acid Fe^{2+} , so the competitive adsorption ability of $(\text{C}_2\text{H}_5)_2\text{NCSS}^-$ in DDTC is stronger than CH_3COO^- . DDTC has a smaller molecular structure than CTAB, so it could supplant more CH_3COO^- adsorbed on the surface of CRS. The molecular structure of DDTC is also larger than Br^- , further increasing the coverage of the surface, leaving the inhibition rate much larger than CTAB. Due to the molecular structure of DDTC is too large, it was difficult to break though the water dipole remained on the surface of CRS. The above reasons resulted in the inhibition rate of DDTC was much higher than the CTAB but not very high.

When the mixed solution of CTAB and DDTC was added into the acetic acid system, Br^- broken through the water dipole layer and produced specific adsorption on the surface of CRS, then played a guiding role in deed. Br^- in the CTAB first broken through the water dipole layer, followed by the $(\text{C}_2\text{H}_5)_2\text{NCSS}^-$ in the DDTC breaking the water dipole layer along the channel which opened by Br^- , and then $(\text{C}_2\text{H}_5)_2\text{NCSS}^-$ instead of CH_3COO^- adsorbed on the surface of CRS. At this point, the $\text{C}_{19}\text{H}_{42}\text{N}^+$ in CTAB tightly adsorbed outside the $(\text{C}_2\text{H}_5)_2\text{NCSS}^-$ layer which adsorbed on the surface of CRS. $\text{C}_{19}\text{H}_{42}\text{N}^+$ and $(\text{C}_2\text{H}_5)_2\text{NCSS}^-$ formed a layer of dense protective film adsorbed on the surface of CRS, and eventually CH_3COO^- was squeezed out, so that the inhibition rate doubled. Electrochemical measurements, FT-IR and SEM also confirm the above theory. Therefore, it can be concluded that the nature of the synergy comes from the synergy between the Br^- in CTAB and the $(\text{C}_2\text{H}_5)_2\text{NCSS}^-$ in DDTC, Br^- can play a guiding role in the presence of $(\text{C}_2\text{H}_5)_2\text{NCSS}^-$. Secondly, it comes from the synergistic adsorption between the $\text{C}_{19}\text{H}_{42}\text{N}^+$ in CTAB and the $(\text{C}_2\text{H}_5)_2\text{NCSS}^-$ in DDTC.

DDTC and CTAB did not affect the mechanism of cathodic and anodic corrosion after synergized, but the corrosion potential shifted 70mV, indicating that the physical adsorption based cover is geometrically cover. This cover makes the anode reaction more difficult to carry out, that is, the particles adsorbed on the surface of the CRS did not participate in the electrode reaction, but their adsorption changes the potential distribution in the electric double layer, which mainly increases the activation energy of the anode corrosion reaction. At the same time, the particles adsorbed on the surface of the CRS isolated the contact between acetic acid and the surface of the CRS, thus affecting the concentration of the particles involved in the corrosion reaction on the surface of the CRS, thus

further slowing down the corrosion rate. This is consistent with the corrosion mechanism we analyzed above.

In previous studies, people also used halide ions as a bridge to make cationic surfactants CTAB adsorb on the surface of CRS [31]. In our study, we used not only “bridge” theory but also HSAB principle when we synergized anionic surfactant DDTC and cationic surfactants CTAB, and our study has a better inhibition efficiency as well.

5. CONCLUSIONS

(1) The corrosion inhibition rate for CRS in 0.05 M HAc is not high when only CTAB or DDTC existed. There is a good synergistic effect between CTAB and DDTC. When the compound ratio is 1:1 (50mg/L:50mg/L), the synergistic inhibition effect is the most obvious, and the inhibition rate after synergized is 86.29%.

(2) The Br⁻ in CTAB opens the channel that allows DDTC to adsorb on the surface of the CRS and then the CTAB adsorbed on the outside of the DDTC by electrostatic adsorption. At last, the CTAB and DDTC form a dense protective film cover the surface of the CRS.

(3) CTAB and DDTC after synergized are adsorbed on the surface of CRS in the form of physical adsorption, and have no effect on the mechanism of cathodic and anodic corrosion.

ACKNOWLEDGEMENT

This work was financially supported by Natural Science Fund Item of China (51561032).

References

1. M. Lagrenée, B. Mernari, M. Bouanis, M. Traisnel and F. Bentiss, *Corros. Sci.*, 44 (2002) 573.
2. G. A. Zhang and Y. F. Cheng, *Corros. Sci.*, 51 (2009) 87.
3. M. A. Veloz and I. González, *Electrochim. Acta*, 48 (2002) 135.
4. C. Schillmoller, Selection and use of stainless steels and nickel-bearing alloys in organic acids, Nickel Development Institute, Toronto, Canada, 1992, 10063.
5. M. A. Quraishi and H. K. Sharma, *J. Appl. Electrochem.*, 35 (2005), 33.
6. C. Zhang and J. M. Zhao, *Acta Phys.-Chim. Sin.*, 30 (2014) 677.
7. Z. W. Wang, W. Bai, Y. Yang, Y. Wu, C. W. Su and J. M. Guo, *Int. J. Electrochem. Sci.*, 11 (2016) 6110.
8. L. G. Qiu, Y. Wu, Y. M. Wang and X. Jiang, *Corros. Sci.*, 50 (2008) 576.
9. P. C. Okafor and Y. Zheng, *Corros. Sci.*, 51 (2009) 850.
10. G. Mu, X. Li and G. Liu, *Corros. Sci.*, 47 (2005) 1932.
11. H. Vashisht, I. Bahadur, S. Kumar, G. Singh, D. Ramjugernath and E. Ebenso, *Int. J. Electrochem. Sci.*, 9 (2014) 5204.
12. A. A. Farag and M. Hegazy, *Corros. Sci.*, 74 (2013) 168.
13. R. Solmaz, M. Mert, G. Kardaş, B. Yazici and M. Erbil, *Acta Phys.-Chim. Sin.*, 24 (2008) 1185.
14. Y. Garsany, D. Pletcher, D. Sidorin and W. Hedges, *Corrosion*, 60 (2004) 1155.
15. D. Pletcher, D. Sidorin and B. Hedges, *Corrosion*, 63 (2007) 285.
16. K. George and S. Nešić, *Corrosion*, 63 (2007) 178.

17. Q. Qu, S. Jiang, L. Li and W. Bai, *Corros. Sci.*, 50(2008) 35.
18. M. A. Amin, S. S. A. El-Rehim, E. El-Sherbini and R. S. Bayoumi, *Electrochim. Acta*, 52 (2007) 3588.
19. X. H. Li, S. D. Deng, H. Fu and G. N. Mu, *J. Appl. Electrochem.*, 39 (2009) 1125.
20. M. Bouklah, B. Hammouti, M. Lagrenee and F. Bentiss, *Corros. Sci.*, 48 (2006) 2831.
21. L. Larabi, Y. Harek, M. Traisnel and A. Mansri, *J. Appl. Electrochem.*, 34 (2004) 833.
22. S. A. Head, W. Q. Shi, E. J. Yang, B. A. Nacev, S. Y. Hong, K. K. Pasunooti, R. J. Li, J. S. Shim and J. O. Liu, *ACS Chem. Biol.*, 12 (2016) 174.
23. S. A. Umoren and M. M. Solomon, *J. Environ. Chem. Eng.*, 5 (2017) 246.
24. M. Morad, *Corros. Sci.*, 42 (2000) 1307.
25. W. Badawy, K. M. Ismail and A. M. Fathi, *Electrochim. Acta*, 51 (2006) 4182.
26. M. Mobin and M. Rizvi, *Carbohydr. Polym.*, 156 (2017) 202.
27. H. Vashisht, S. Kumar and I. Bahadur, *Int. J. Electrochem. Sci.*, 8 (2013) 684.
28. L. Y. S. Helen, A. A. Rahim and B. Saad, *Int. J. Electrochem. Sci.*, 9 (2014) 830.
29. P. K. Chattaraj and B. Maiti, *J. Am. Chem. Soc.*, 125 (2003) 2705.
30. G. Mu, T. Zhao, M. Liu and T. Gu, *Corrosion*, 52 (1996) 853.
31. X. Li, L. Tang, H. Liu, G. Mu and G. Liu, *Mater. Lett.*, 62 (2008) 2321.

© 2017 The Authors. Published by ESG (www.electrochemsci.org). This article is an open access article distributed under the terms and conditions of the Creative Commons Attribution license (<http://creativecommons.org/licenses/by/4.0/>).